

# 1 High-resolution global shipping emission inventory by 2 Shipping Emission Inventory Model (SEIM)

3 Wen Yi <sup>1</sup>†, Xiaotong Wang <sup>2</sup>†, Tingkun He <sup>1</sup>, Huan Liu <sup>1</sup>\*, Zhenyu Luo <sup>1</sup>, Zhaofeng Lv  
4 <sup>1</sup>, Kebin He <sup>1</sup>

5 <sup>1</sup> State Key Joint Laboratory of ESPC, School of Environment, Tsinghua University, Beijing 100084,  
6 China

7 <sup>2</sup> Key Laboratory of Beijing on Regional Air Pollution Control, Beijing University of Technology,  
8 Beijing 100124, China

9 \* Correspondence to: liu\_env@tsinghua.edu.cn (H. Liu)

10 † These authors contributed equally to this work

11 **Abstract:** The high-resolution ship emission inventory serves as a crucial dataset for various disciplines  
12 including atmospheric science, marine science, environmental management, etc. Here, we present a  
13 global high spatiotemporal resolution ship emission inventory at a resolution of  $0.1^\circ \times 0.1^\circ$  for the years  
14 2013, 2016-2021, generated by the state-of-the-art Shipping Emission Inventory Model (SEIMv2.2).  
15 Initially, the annual 30 billion Automatic Identification System (AIS) data underwent extensive cleaning  
16 to ensure data validity and accuracy in temporal and spatial distribution. Subsequently, integrating real-  
17 time vessel positions and speeds from AIS data with static technical parameters, emission factors, and  
18 other computational parameters, SEIM simulated ship emissions on a ship-by-ship, signal-by-signal basis.  
19 Finally, the results were aggregated and analyzed. In 2021, the ship activity dataset established based on  
20 AIS data covered 109.3 thousand vessels globally (101.4 thousand vessels reported by the United Nations  
21 Conference on Trade and Development). Concerning the major air pollutants and greenhouse gases,  
22 global ships emitted 847.2 million tons of CO<sub>2</sub>, 2.3 million tons of SO<sub>2</sub>, 16.1 million tons of NO<sub>x</sub>, 791.2  
23 kilo tons of CO, 737.3 kilo tons of HC ([Hydrocarbon](#)), 415.5 kilo tons of primary PM<sub>2.5</sub>, 61.6 kilo tons  
24 of BC ([black carbon](#)), 210.3 kilo tons of CH<sub>4</sub>, 45.1 kilo tons of N<sub>2</sub>O in 2021, accounting for 3.2% of SO<sub>2</sub>,  
25 14.2% of NO<sub>x</sub>, and 2.3% of CO<sub>2</sub> emissions from all global anthropogenic sources, based on the  
26 Community Emissions Data System (CEDS). Due to the implementation of fuel-switching policies,  
27 global ship emissions of SO<sub>2</sub> and primary PM<sub>2.5</sub> saw a significant reduction of 81.3% and 76.5% in 2021  
28 compared to 2019, respectively. According to the inventory results, the composition of vessel types  
29 contributing to global ship emissions remained relatively stable through the years, with container ships

30 consistently contributing ~ 30% of global ship emissions. Regarding vessel age distribution, the emission  
31 contribution of vessels built before 2000 (without Tier standard) has been declining, dropping to 10.2%  
32 in 2021, suggesting that even a complete phase-out of these vessels would have limited potential for  
33 reducing NOx emissions in the short term. On the other hand, the emission contribution of vessels built  
34 after 2016 (meeting Tier III standard) kept increasing, reaching 13.3% in 2021. Temporally, global ship  
35 emissions exhibited minimal daily fluctuations. Spatially, high-resolution emission characteristics of  
36 different vessel types were delineated. Patterns of ship emission contributions by different types of  
37 vessels vary among maritime regions, with container ships predominant in the North and South Pacific,  
38 bulk carriers predominant in the South Atlantic, and oil tankers prevalent in the Arabian Sea. The  
39 distribution characteristics of ship emissions and intensity also vary significantly across different  
40 maritime regions. Our dataset, which is accessible at <https://zenodo.org/records/11069531> (Wen et al.,  
41 2024), provides daily breakdown by vessel type and age is available for broad research purposes, and it  
42 will provide a solid data foundation for fine-scale scientific research and shipping emission mitigation.

## 43 **1 Introduction**

44 Ships carry over 80% of global trade volume (Development, 2023). Employing heavy fuel oil, ships  
45 emit significantly more atmospheric pollutants than diesel cars each year (Corbett et al., 1999; Endresen  
46 et al., 2003; Jasper Faber, 2020). Existing studies indicate that ship emissions of atmospheric pollutants  
47 and greenhouse gases have important environmental and climatic impacts on multiple spheres of the  
48 Earth (Browse et al., 2013; Chen et al., 2020; Diamond, 2023; Zhang et al., 2021). In terms of air quality,  
49 ships are regarded as a major source of PM<sub>2.5</sub> pollution in coastal cities (Liu et al., 2024; Luo et al., 2023).  
50 Recent studies show that although ship emissions have decreased due to stricter control measures in  
51 recent years, shipping-related mortality associated with long-term PM<sub>2.5</sub> exposure in Chinese coastal  
52 areas increased by 11.4% from 2016 to 2020 as populations migrate towards coastal cities (Luo et al.,  
53 2024). Ship emission-induced sulfur oxides aerosols, significantly influence local climates (Liu et al.,  
54 2016; Yuan et al., 2022). With the increasing navigation in the Arctic, ship emissions of black carbon  
55 have become a focal point of research and policy debates regarding their impact on the polar ice surface  
56 (Stephenson et al., 2018; Zhang et al., 2019). Regarding their impact on marine organisms, anthropogenic

57 emissions account for over 80% of the utilizable nitrogen deposition in the ocean, with maritime  
58 emissions contributing to 15% of global NO<sub>x</sub> emissions (Zhang et al., 2021). Given these facts,  
59 characterizing ship emissions is crucial for fundamental research in atmospheric, marine, and climatic  
60 sciences, etc.

61 The characterization of ship emissions through emission inventories stands as a pivotal and effective  
62 methodology within maritime emissions research (Liu et al., 2016; Liu et al., 2024; Wang et al., 2021).  
63 Over the past 30 years, with the improvement of ship activity data collection mechanisms, the  
64 establishment of ship emission inventories has gradually shifted from the "top-down" approach, based  
65 on fuel or power consumption statistics and empirical parameters, to the "bottom-up" approach, based  
66 on high spatiotemporal resolution shipping trajectory data (Eyring et al., 2010; Jasper Faber, 2020; Liu  
67 et al., 2016). Currently, the establishment of high spatiotemporal resolution ship emission inventories  
68 based on Automatic Identification System (AIS) data has become the most popular tool for scientific  
69 research and policy management in the field of ship emissions (Johansson et al., 2017; Kramel et al.,  
70 2021; Wang et al., 2021). AIS consists of onboard equipment, shore-based and satellite-based receivers.  
71 During navigation, the onboard equipment transmits AIS signals every 2 seconds to several minutes,  
72 which are received by terrestrial or satellite-based AIS receivers and then transmitted in-time to servers  
73 for storage. AIS messages record the ship's unique identifier and high-frequency dynamic information  
74 that changes continuously as the vessel progresses, including the vessel's MMSI code, IMO number,  
75 signal transmission time, ship's position (longitude and latitude), over-ground speed, operational status,  
76 draft, and destination, among others. Leveraging real-time ship speed derived from AIS data along with  
77 vessel technical specifications such as deadweight tonnage and design speed, and emission factors, it is  
78 feasible to model instantaneous ship emissions and then aggregate them at a defined spatiotemporal  
79 granularity, thereby constructing a high-resolution emission inventory dataset. The advantage of this  
80 method is that the derived emission inventory does not rely on external spatiotemporal allocation  
81 parameters, but retains accurate spatiotemporal information of ship emissions from AIS data (Liu et al.,  
82 2016). However, the challenge lies in the difficulty of processing AIS data, the complexity of simulating  
83 instantaneous ship emissions, and the significant computational resources required (Chen and Yang,  
84 2024). Currently, the mainstream international ship emission inventory models based on AIS data include  
85 the Ship Traffic Emission Assessment Model (STEAM)(Jalkanen et al., 2012; Johansson et al., 2017) ,

86 the Shipping Emission Inventory Model (SEIM), International Maritime Organization (IMO) emission  
87 inventory model (Jasper Faber, 2020), Maritime Transport Environmental Assessment Model  
88 (MariTEAM) (Kramel et al., 2021), etc.

89 In this study, we established a  $0.1^\circ \times 0.1^\circ$  global daily ship emission inventory for the years 2013,  
90 2016-2021 based on SEIMv2.2. This dataset covers five air pollutants ( $\text{NO}_x$ ,  $\text{SO}_2$ ,  $\text{PM}_{2.5}$ ,  $\text{CO}$ ,  $\text{HC}$ ) and  
91 four greenhouse gases ( $\text{CO}_2$ ,  $\text{CH}_4$ ,  $\text{N}_2\text{O}$ ,  $\text{BC}$ ). Due to rigorous quality control, the ship emission inventory  
92 established by SEIM possesses high information density, allowing for analysis across multiple  
93 dimensions, such as fleet structure and spatiotemporal characteristics. Initially, we conducted meticulous  
94 data cleaning and rigorous quality control on the commercially obtained global ship AIS data to establish  
95 a reliable ship activity dataset. Subsequently, employing the latest emission factor and real-time engine  
96 power simulation methods for ships, SEIMv2.2 computed instantaneous ship emissions, integrating  
97 multiple quality control techniques such as interpolation processing for sparse routes and safety margin  
98 considerations to ensure the accuracy of ship emission simulation. Finally, we aggregated ship emissions  
99 from different temporal and spatial scales, as well as from different types and ages of ships. The derived  
100 high-resolution global shipping emission inventory could serve as input data for climate or atmospheric  
101 chemistry models.

102 The next section will elucidate the methodology and factors employed in establishing our high-  
103 resolution ship emission inventory. Section 3.1 compares our results with previous global ship emission  
104 inventories. Section 3.2 analyzes the temporal sequence of global ship emissions. Section 3.3 examines  
105 the spatial distribution characteristics of global ship emissions. Section 4 provides information regarding  
106 our dataset and data availability. Finally, Section 5 presents the conclusion.

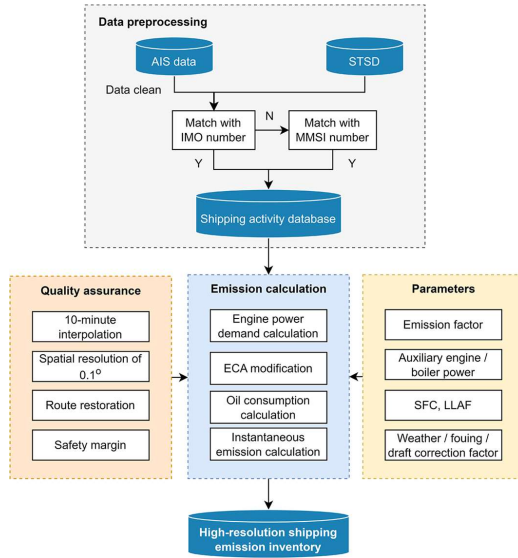
## 107 **2 Methods**

### 108 **2.1 Ship Emission Inventory Model (SEIM)**

#### 109 **2.1.1 General principles**

110 The Shipping Emission Inventory Model (SEIM) was first established by (Liu et al., 2016) based on the  
111 idea of disaggregated dynamic method. Driven by AIS data, combined with each vessel's registration  
112 information, SEIM realized real-time, vessel-by-vessel shipping emission simulations. SEIM is suitable

113 for the establishment of multi-scale shipping emission inventories with applications on regions (Liu et  
114 al., 2016; Wang et al., 2021) and ports (Fu et al., 2017). SEIM has undergone two major updates:  
115 SEIMv2.0 (Wang et al., 2021) and SEIMv2.2 (this study). Compared to SEIMv2.0, SEIMv2.2 features  
116 three key improvements. (1) IMO numbers are employed as the primary identifier to match AIS data and  
117 Ship Technical Specifications Database (STSD), and for those that cannot be matched, MMSI ([Maritime](#)  
118 [Mobile Service Identity](#)) codes are used as the secondary identifier. We found that the matching rate of  
119 the ship archive database established in previous years could significantly decrease when applied to new  
120 years. This is because when ships are leased or AIS equipment is replaced, the MMSI code often changes,  
121 while the IMO code remains constant. Therefore, using the IMO code as the first-choice identifier ensures  
122 more accurate matching of AIS data and static ship information. See Sect. 2.1.2 for details. (2) The  
123 formula for calculating the main engine load has been revised to include parameterized correction  
124 schemes for draft, meteorological conditions, and hull fouling. Additionally, a main engine load  
125 maximum limit of 98% is set to consider the navigation safety of ships. Refer to Sect. 2.1.3 for further  
126 details. (3) The ship emission factors are comprehensively updated according to the Fourth Green House  
127 Gases Study by IMO (Jasper Faber, 2020), and a black carbon calculation module has been integrated.  
128 This update also integrates the Emission Control Area (ECA) module correction module directly into the  
129 calculation process, rather than applying it as a post-process adjustment. Detailed methods are provided  
130 in Sect. 2.1.4. During the development of SEIMv2.2, SEIMv2.1 was derived, which only updated the  
131 emission factors compared to SEIMv2.0. Generally, the technical scheme of SEIMv2.2 is illustrated in  
132 Fig. 1.



133

134 **Figure 1: The technical scheme for SEIMv2.2**

135 The calculation process and principles of SEIMv2.2 could be described as follows: Firstly, the original  
 136 AIS data collected are subjected to cleaning, missing data filling, etc., to establish a well-cleaned dynamic  
 137 AIS database. Secondly, IMO or MMSI codes are used as unique identifiers to match AIS data with the  
 138 STSD, which provides essential technical parameters such as vessel type, deadweight tonnage, main  
 139 engine power rating, design speed, etc., to establish a comprehensive shipping activity database. For the  
 140 details of STSD, refer to (Wang et al., 2021). This study has incorporated information on newly built  
 141 vessels from 2019 to 2021, obtained from the Lloyd's Register, into the established STSD. Thirdly, a  
 142 series of parameters such as emission factors, auxiliary engine and boiler output power, specific fuel  
 143 consumption, low load adjustment factors, and weather and fouling factors are input for ship emission  
 144 simulation. Then, the model will calculate GHGs (Greenhouse gases) and air pollutant emissions for  
 145 every ship by every two subsequent AIS signals. The emissions from the main engine, auxiliary engine,  
 146 and boiler are simulated using the corresponding formulas presented as Equation (1) - (3).

$$E_{ME,i,n,p} = P_{ME,i,n} \times EF_{ME,i,p} \times LLAF_{i,n,p} \times \Delta T_{i,n} \times 10^{-6} \quad (1)$$

147

$$E_{AE,i,n,p} = P_{AE,i,n} \times EF_{AE,i,p} \times \Delta T_{i,n} \times 10^{-6} \quad (2)$$

148

$$E_{B,i,n,p} = P_{B,i,n} \times EF_{B,i,p} \times \Delta T_{i,n} \times 10^{-6} \quad (3)$$

149 Where the subscripts ME, AE, and B represent the main engine, auxiliary engine, and boiler, respectively;  
 150  $i$  represents individual ship;  $n$  represents the  $n$ -th AIS signals in the sequence, and the total number of  
 151 AIS signals transmitted by the ship  $i$  could be expressed using  $N_i$ ;  $p$  represents species of GHGs or air  
 152 pollutants. As for the capital letters,  $E$  represents the emissions of GHGs or air pollutants (unit: ton);  $EF$   
 153 is the emission factors (unit: g/kwh);  $P$  is the output power (unit: kw);  $\Delta T$  is the time interval of two  
 154 subsequent AIS signals (unit: h); LLAF is the low load adjust factor, which is applied only when the  
 155 main engine load factor is lower than 20%, consistent with our previous work. The total emissions are  
 156 calculated by summing up the emissions from all main engines, auxiliary engines, and boilers, as shown  
 157 in Equation (4).

$$E_{i,p} = \sum_{n=1}^{N_i-1} E_{i,n,p} = \sum_{n=1}^{N_i-1} (E_{ME,i,n,p} + E_{AE,i,n,p} + E_{B,i,n,p}) \quad (4)$$

158 During the real-time calculation, linear interpolation is applied to latitude and longitude displacement as  
 159 well as time intervals where the AIS time interval is greater than ten minutes. AIS latitude and longitude  
 160 are rounded to one decimal place to ensure a spatial resolution of  $0.1^\circ \times 0.1^\circ$ . In the Chinese coastal  
 161 region, route restoration technology is applied to restore routes crossing land, referred to (Wang et al.,  
 162 2021). If, due to anomalies in speed or other factors, the main engine load exceeds 100%, it is capped at  
 163 98% for safety navigation considerations. Finally, the high-resolution emission inventory generated by  
 164 SEIM could be aggregated and analyzed from various angles such as emission structure, temporal  
 165 variations, spatial distribution, etc., depending on study demands.

166 **2.1.2 AIS data cleaning**

167 AIS data provide high-density vessel activity data, including time, speed, and latitude-longitude  
168 coordinates. This study collected global shore-based and satellite-based AIS data, with an average annual  
169 signal count of approximately 30 billion. Due to irregular or erroneous information entry at ports or on  
170 vessels, as well as interference from complex marine environments, weather conditions, and terrain, AIS  
171 data may suffer from errors, duplicates, and losses. To enhance the accuracy of emission inventory  
172 calculations, this study conducted meticulous cleaning of AIS data. Firstly, to ensure data validity, we  
173 filter AIS message records that met all of the following conditions: 1) Annual AIS signal count greater  
174 than 10; 2) Speed over ground less than 50 knots; 3) Longitudes ranged from  $-180^{\circ}$  to  $180^{\circ}$  and latitudes  
175 ranged from  $-90^{\circ}$  to  $90^{\circ}$ ; 4) The timestamp of AIS signals within the target year.

176 Secondly, for temporal anomaly cleaning, signals with excessively long time intervals are filtered  
177 out. According to the International Convention for the Safety of Life at Sea (SOLAS), vessels are  
178 required to maintain continuous transmission of AIS signals throughout the year, except for specific  
179 reasons permitted by regulations. Therefore, vessels theoretically maintain a high frequency of signal  
180 transmission during navigation. Taking the year 2021 as an example, Fig. S 3 reveals a distinct bimodal  
181 distribution of original AIS signals, with peaks occurring around 300 seconds and 2 hours. The peak of  
182 around 300 seconds corresponds to the high-frequency interval for shore-based AIS equipment to receive  
183 signals, while the peak of around 2 hours mainly originates from satellite AIS signals. Statistical analysis  
184 shows that 99.6% of signal time intervals are within 8000 seconds. However, the total duration of these  
185 AIS signal intervals accounts for only 16% of all AIS signals, indicating the presence of extremely long  
186 consecutive signal intervals in the AIS data. This may be due to vessel docking for repairs or AIS  
187 equipment malfunctions. To minimize uncertainty in emission calculations caused by these signals, this  
188 study filters out signals with time intervals exceeding 7 days, which are not included in the emission  
189 calculations.

190 Thirdly, for spatial distribution anomalies cleaning, AIS data distributed on land are filtered out.  
191 Spatial distribution of the annual original AIS signal (Fig. S 4) revealed a significant number of signals  
192 deviating from shipping routes near the  $0^{\circ}$  and  $120^{\circ}$  meridians, located over Asia, Europe, and Africa.  
193 Further analysis indicated that such abnormal signal points are caused by misaligned field information  
194 or data loss. To minimize the interference of these abnormal signals on emission calculations, this study



195 employs the following cleaning methods: 1) For ships matched by IMO codes, signals with speeds >50  
196 knots or consecutive latitude-longitude spans >20° are removed; 2) For ships matched by MMSI codes,  
197 signals with speeds >40 knots or latitude-longitude spans >8° are excluded; 3) Signals located on land  
198 areas are excluded. Fig. S 4 simultaneously presents the spatial distribution of the cleaned AIS signals,  
199 revealing that signals on land near the 0° and 120° meridians have been eliminated while retaining signals  
200 on major navigable rivers in North America, South America, and Eurasia.

201 Fourthly, to ensure the reliability of ship technical parameter data matching, the AIS data are  
202 subsequently aggregated and identified with IMO numbers and MMSI numbers. AIS data comprises  
203 static AIS data and dynamic AIS data. Static AIS data include time, MMSI numbers, IMO numbers, etc.,  
204 but do not contain latitude and longitude information. Dynamic AIS data contain MMSI numbers and  
205 latitude and longitude information. This study integrates the static AIS data and dynamic AIS data by  
206 matching their common MMSI numbers. It is found that approximately 84% of the MMSI numbers in  
207 dynamic information could be matched with a unique valid seven-digit IMO number. However, some  
208 ships may change their MMSI codes multiple times within a year. Data with MMSI code changes more  
209 than 10 times are excluded from emission calculations.

### 210 **2.1.3 Engine power demand**

211 Engine power demand is crucial for emission calculations. For the main engine, its real-time output  
212 power is related to the main engine load, which can be depicted in real-time by changes in the ship's  
213 speed-over-ground obtained from AIS data. According to the propeller law, the main engine load factor  
214 is the cube of the ratio of the ship's actual speed to its design speed (Liu et al., 2016). Additionally, some  
215 studies indicate that factors such as draft, hydrological and weather conditions, and hull fouling also  
216 influence the main engine load (Chen and Yang, 2024; Emmens et al., 2021; Fu et al., 2022). Regarding  
217 draft factors, the (Jasper Faber, 2020) corrects the main engine load using real-time draft data from AIS.  
218 However, draft fields in commercial AIS data are often manually recorded by crew members, leading to  
219 low accuracy and a large number of zero values. As for hydrological and weather conditions, wind and  
220 waves could increase engine power demand through friction and shear resistance. (Johansson et al., 2017)  
221 adopts a method based on a real-time ship heading and weather field, which requires substantial  
222 computational resources and introduces greater uncertainty by the weather field. Additionally, the

223 accumulation of micro- and macro-organisms on ship surfaces increases power demand to overcome  
 224 resistance, and existing studies often use fixed parameters to correct the influence. This study introduces  
 225 parameterization schemes to correct the influence of draft, weather, and hull fouling. Based on the ships'  
 226 payload utilization calculation algorithm in (IMO, 2015), this study estimates the average drafts for  
 227 different types of vessels, with specific values provided in Table S1. The correction coefficients for  
 228 weather influences ( $\eta_w$ ) are based on (Jasper Faber, 2020), also presented in Table S1. The correction  
 229 coefficient for fouling influences ( $\eta_f$ ) is set to 0.917. Specifically, the formula for calculating the real-  
 230 time power of the main engine in SEIMv2.2 can be found in equation (5).

$$P_{ME,i,n} = P_{ref,i} \times LF_{i,n} = \frac{P_{ref,i} \times \left(\frac{D_i}{D_{ref,i}}\right)^{0.66} \times \left(\frac{v_{i,n}}{v_{ref,i}}\right)^3}{\eta_w \times \eta_f} \quad (5)$$

231 Where  $P_{ref,i}$  represents the maximum engine output power (unit: kw) of the main engine of the  
 232 ship  $i$ ;  $LF_{i,n}$  represents the main engine load factor of the ship  $i$  at the  $n$ -th AIS signals in the sequence.  
 233  $D_i$  represents the average draft;  $D_{ref,i}$  represents the designed draft;  $v_{i,n}$  represents the speed-over-  
 234 ground (unit: knot) of the ship  $i$  at the  $n$ -th AIS signals in the sequence;  $v_{ref,i}$  represents the design  
 235 speed (unit: knot) of ship  $i$ , obtained from the static technical profiles;  $\eta_{w,i}$  represents the weather  
 236 correction factor and  $\eta_{f,i}$  represents the fouling correction factor, both of which are unitless.

237 For auxiliary engines and boilers' power demand, this study adopts the recommended values from the  
 238 IMO Fourth and Third Greenhouse Gas Study reports. Due to the lack of information, this study did not  
 239 consider the impact of other auxiliary devices on board, such as solar panels, wind sails, waste heat  
 240 recovery systems, and carbon capture, utilization and storage (CCUS) systems, on vessel energy  
 241 consumption. These systems are not significant contributors to overall vessel energy consumption  
 242 currently (Dnv, 2022). However, with the ongoing trends of energy efficiency improvements, the impact  
 243 of these systems on vessel energy utilization could be transformative in the future (Kersey et al., 2022).

#### 244 2.1.4 Emission factors

245 The emission factors applied by SEIMv2.0 is mainly based on the Third IMO GHG Study (Smith,  
 246 2014) as well as the National Standard for General Diesel Fuel of the People's Republic of China (Wang  
 247 et al., 2021). In this study, we updated the emission factors based on the Forth IMO GHG Study (Jasper

248 Faber, 2020), and therefore accompanying technical modification. Firstly, emission factors of  
 249 conventional air pollutants (SO<sub>2</sub>, NO<sub>x</sub>, PM<sub>2.5</sub>, CO, HC) and GHGs (CO<sub>2</sub>, CH<sub>4</sub>, N<sub>2</sub>O) were updated. CO<sub>2</sub>,  
 250 SO<sub>2</sub>, and PM<sub>2.5</sub> are considered typical species whose emission factors are highly dependent on the  
 251 chemical component of fuels. Table. S2 represents the emissions factors based on fuel consumption for  
 252 CO<sub>2</sub>, SO<sub>2</sub>, and PM<sub>2.5</sub>. Energy-based emission factors are calculated based on fuel-based emission factors  
 253 as well as specific fuel consumptions (SFC, unit: kwh/kg fuel), using Equation (6):

$$EF_e = EF_f \cdot SFC \quad (6)$$

254 SFC represents the fuel consumption per unit of work performed by a ship, mainly decided by the  
 255 fuel calorific value (kwh/kg fuel) and engine efficiency (%). During the operation of ships, energy  
 256 efficiency could be considered as a quadratic function of the load factor of the main engine, generally  
 257 with the optimal load factor of 80%. Equation (7) is applied to calculate the SFC for main engines based  
 258 on the SFC under the optimal operating condition ( $SFC_{base}$ ) and main engine load of the ship  $i$ .

$$SFC_{ME,i} = SFC_{base,ME,i} \cdot (0.455 \cdot LF_i^2 - 0.71 \cdot LF_i + 1.28) \quad (7)$$

259 Generally, newer ships have a lower  $SFC_{base}$  than older ships due to the improvement of engine  
 260 and auxiliary engine efficiency (Sou et al., 2022). The LNG fleet also has a lower  $SFC_{base}$  value than  
 261 conventional fuel. SFC of auxiliary engines and boilers ( $SFC_{AE|B,i}$ ) is not subject to the main engine load,  
 262 so  $SFC_{AE|B,base,i}$  is directly applied with no main engine load adjustment. Values of  $SFC_{base}$  are  
 263 exhibited in Table. S 3.

264 Combining Table. S 2 and Equations (1), and (2), energy-based emission factors for the main  
 265 engines of CO<sub>2</sub> and SO<sub>2</sub> as a function of the main engine load could be derived, as exhibited in Fig. S 1.  
 266 It could be noted that although Marine Gas Oil (MGO) has a higher carbon content compared to Heavy  
 267 Fuel Oil (HFO), its lower SFC results in a lower energy-based CO<sub>2</sub> emission factor. Fig. S 2 illustrates a  
 268 comparison between two algorithms employed in SEIMv2.0, which utilizes uniform emission factors for  
 269 all operational conditions, and SEIMv2.2, which incorporates load-dependent emission factors. We  
 270 selected a typical oil tanker with dead-water tonnage of 7562 tons and examined its hourly carbon  
 271 emissions from July 1 to July 15, 2019. It is evident that, at anchorage or berth, the hourly emissions

272 estimated by SEIMv2.2 are generally higher than or equal to those of the previous SEIMv2.0. When the  
273 vessel is cruising, however, the overall emissions calculated by SEIMv2.2 are relatively lower compared  
274 to SEIMv2.0. Emission factors of other air pollutants and GHGs in this study are shown in Table S 4 and  
275 Table S 5.

## 276 **2.2 Data source and quality control**

### 277 **2.2.1 AIS data coverage**

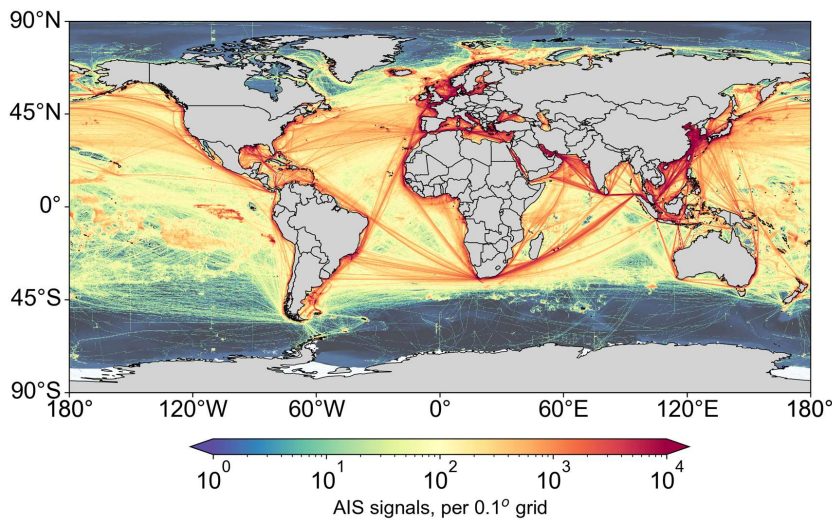
278 The AIS-observed data obtained in this study amounted to approximately 30 billion/year, while the  
279 processed AIS signals after cleaning and interpolation averaged about 4-5 billion per year, with an  
280 average annual operating time of approximately 5-7 million hours, as shown in Table 1. In comparison  
281 to (Johansson et al., 2017), the AIS signal volume in this research is slightly lower, possibly due to  
282 comprehensive quality control measures in data reduction and filtering, which removed a significant  
283 number of signals with inadequate validity, abnormal time or spatial distribution, and insufficient  
284 reliability. It can be observed that with the increasing prevalence of AIS equipment, the quantity of AIS  
285 signals is on the rise. However, the operating time does not necessarily increase in proportion to the  
286 signal quantity. The operating time decreased by 3.8% in 2020 compared to 2019 and increased by 4.5%  
287 in 2021 compared to 2020, probably influenced by the pandemic,  
288

289 **Table 1: Annual AIS signals and operating time after data cleaning**

Year	2013	2016	2017	2018	2019	2020	2021
AIS signals, billion	1.6	4.1	4.6	5.0	5.0	5.0	5.5
Operating time, million hour	225.8	578.5	643.6	700.9	693.8	667.3	697.6

290

291 Taking 2021 as an example, the spatial distribution of AIS signals after cleaning and time interpolation  
 292 is illustrated in Fig. 2. The spatial coverage of cleaned AIS signals is extensive, with signals primarily  
 293 concentrated along major shipping routes such as the coastal regions of East Asia, the Malacca Strait-  
 294 Cape of Good Hope route, the Mediterranean, and the Black Sea routes, effectively depicting the  
 295 trajectories of major shipping lanes.



296

297 **Figure 2: The spatial distribution of global AIS signals in 2021. Maps are made with Natural Earth.**

298

299 **2.2.2 Global fleet composition**

300 Table 2 presents the global fleet structure obtained through matching AIS data with STSD in 2021. This  
 301 study covers 14 vessel types, including major cargo vessels, passenger ships, and fishing vessels, along

302 with a category labeled "others," comprising research vessels, rescue ships, and work vessels, among  
303 others. Since the "others" category primarily consists of small coastal vessels, its contribution to  
304 emissions is minor. It's important to note that United Nations Conference on Trade and Development  
305 (UNCTAD) definition of "others" differs from this study's categorization. According to UNCTAD 2021  
306 classification, other ships include liquefied petroleum gas carriers, liquefied natural gas carriers, parcel  
307 (chemical) tankers, specialized tankers, reefers, offshore supply vessels, tugboats, dredgers, cruise ships,  
308 ferries, and other non-cargo ships. Moreover, it should be noted that the fleet obtained in this study  
309 comprises vessels with certain activity levels (annual AIS signals exceeding 10), whereas UNCTAD  
310 statistics do not consider vessel activity. This discrepancy might lead to comparatively lower results in  
311 this study.

312 Overall, the discrepancies between the global fleet statistics in this study and those of UNCTAD are not  
313 substantial. In terms of vessel numbers, this study reached 109.3 thousand in 2021, slightly higher than  
314 UNCTAD's 101.4 thousand. The total deadweight tonnage amounts to 1989.9 million tons, slightly lower  
315 than UNCTAD's 2136.2 million tons. Among the fleet obtained in this study, vessels matched by IMO  
316 numbers reach 62.9 thousand, contributing 57.5% of vessel count and 95.4% of deadweight tonnage.  
317 Vessels matched by MMSI numbers constitute a larger proportion in count (42.5%), yet make a smaller  
318 contribution in deadweight tonnage (4.6%), predominantly consisting of fishing vessels (which  
319 contribute 87.9% to the vessel count matched by MMSI numbers). There's a noticeable difference in the  
320 quantity of general cargo ships and oil tankers. However, in terms of total tonnage, the container ships,  
321 general cargo ships, bulk carriers, and oil tankers show no significant differences (below 10%) with  
322 UNCTAD, ensuring the reliability of global ship emission calculations and emission structure analysis.  
323

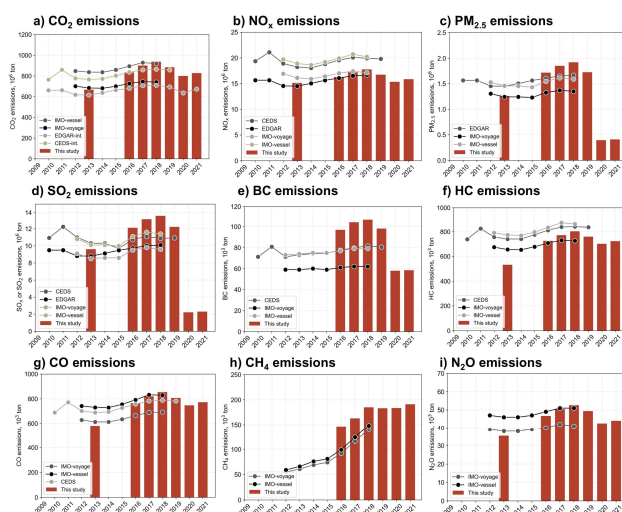
324 **Table 2: Comparison of the global fleet structure of this study and the UNCTAD statistics in 2021. The fleet**  
 325 **analyzed in this study was filtered to include vessels with an annual AIS signal count greater than 10.**

Vessel type	Number of vessels, thousand				Total deadweight tonnage, million ton			
	This study			UNCTAD	This study			UNCTAD
	match with IMO number	match with MMSI number	total		match with IMO number	match with MMSI number	total	
Auto Carrier	0.8	0.1	0.8		15.3	0.9	16.2	
Bulk Carrier	11.1	0.6	11.7	12.3	842.3	27.6	869.9	913.2
Chemical Tanker	4.7	0.3	5.0		100.5	4.5	105.0	
Container	4.2	0.3	4.5	5.4	218.8	14.4	233.2	281.8
Cruise	0.2	0.1	0.2		0.1	0.0	0.1	
Fishing ship	5.1	40.8	45.8		4.0	5.8	9.7	
General Cargo	6.9	0.8	7.7	20.0	66.4	4.4	70.7	77.9
LNG	0.3	0.0	0.3		19.3	0.2	19.5	
LPG	1.2	0.1	1.2		19.0	0.8	19.9	
Miscellaneous	12.3	1.4	13.7		76.1	6.5	82.6	
Ocean Tug	7.0	0.9	7.9		13.4	1.6	15.0	
Oil Tanker	5.4	0.4	5.8	11.5	505.3	22.2	527.5	619.3
Reefer	0.5	0.0	0.5		3.5	0.2	3.7	
Ro Ro	3.0	0.6	3.6		11.8	1.7	13.5	
Others	0.5	0.0	0.5	52.2	3.1	0.0	3.1	243.9
Total	62.9	46.4	109.3	101.4	1899.1	90.8	1989.9	2136.2

326

327 3 Results

328 3.1 Total global shipping emissions



329  
330 **Figure 3: Global trends in shipping emissions from 2010 to 2021.** Data source: IMO (Jasper Faber, 2020),  
331 where IMO-Voyage results were calculated based on a voyage-based method and IMO-Vessel on a vessel-based  
332 algorithm. Community Emissions Data System (McDuffie et al., 2020); Emissions Database for Global  
333 Atmospheric Research (Crippa, 2021).

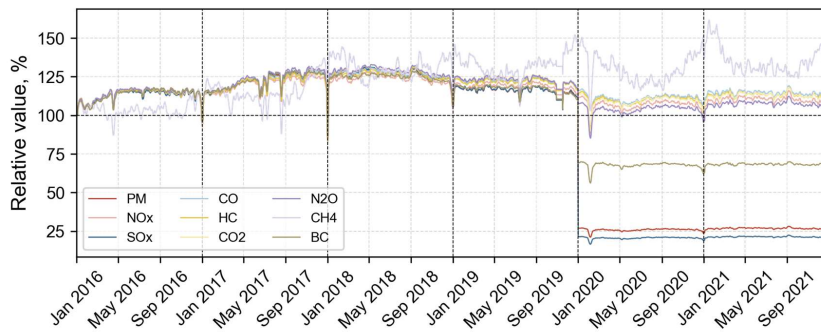
334 We established a multi-year global ship emissions inventory with temporal resolution of day and  
335 spatial resolution of 0.1° using the SEIM model for the years 2013 and 2016-2021. Figure 3 summarizes  
336 this study and open-source dataset of major atmospheric pollutants and greenhouse substances emitted  
337 by global shipping over the past decade. The ship emission calculation method employed in this research,  
338 which is AIS-based, aligns with those utilized in the EDGAR ([Emissions Database for Global](#)  
339 [Atmospheric Research](#)) inventory and the Fourth IMO GHG Study released in 2020, while the CEDS  
340 inventory is established based on a top-down fuel-based approach (McDuffie et al., 2020).  
341 Methodologically, our study is more comparable to the research conducted by EDGAR and IMO, with  
342 the results from the CEDS inventory as a reference. It is important to note that the SEIM model has  
343 undergone two major version updates. The data of different versions are presented in Figure S3. Figure  
344 3 presents the integrated results for ease of comparison with other studies. Specifically, the results for  
345 2013 are based on SEIMv1.0, while those for 2016-2020 are based on SEIMv2.1 and those for 2021 are



346 based on SEIMv2.2. Due to slight differences between the two versions (Fig. S5), both of which include  
347 data for 2020, the total emissions for 2020 in SEIMv2.2 were adjusted to match those in SEIMv2.1. The  
348 growth rate for 2021 was kept consistent to ensure that the data for both versions align in 2020. In terms  
349 of annual emission totals, this study's results show similarities in emission trends and total emissions  
350 compared to well-known inventories such as EDGAR and IMO. For most species, this study's results  
351 show higher annual growth rates compared to IMO and EDGAR studies. For instance, this study  
352 estimates a 6.1% annual increase rate in global ship CO<sub>2</sub> emissions from 2016 to 2018, while IMO's  
353 study indicates only a 1.4% annual increase for its "vessel-based" results and 0.9% for its "voyage-based"  
354 results. In 2019 and 2020, influenced by international trade conflicts and the global pandemic, this study  
355 estimates a 5.8% and 9.5% year-on-year decrease in global ship CO<sub>2</sub> emissions for 2019 and 2020,  
356 respectively. In contrast, the year-on-year decrease rate estimated by EDGAR inventory is 2.1% and 8.4%  
357 for 2019 and 2020, respectively. Differences between studies may stem from factors such as AIS data  
358 quality, coverage of static information, and factors considered in emission calculations. In 2020, the  
359 global implementation of the fuel-switching policy led to a significant reduction in the sulfur content of  
360 ship fuel. According to SEIM, in 2020 relative to 2019, SO<sub>2</sub>, PM<sub>2.5</sub>, and BC emissions decreased by  
361 81.9%, 77.2%, and 40.9%, respectively. In 2021, following the recovery in global trade demand after the  
362 pandemic, this study estimates an increase of 3.5% in global ship CO<sub>2</sub> emissions compared with 2020,  
363 while EDGAR inventory estimates an increase of 5.9%. However, the latest data on ship's atmospheric  
364 pollutants from other inventories only extend to 2019, which is insufficient for comparing emission  
365 results with this study.

366 3.2 Temporal evolutions

367 3.2.1 Daily shipping emissions



368

369 **Figure 4: Daily global shipping air pollutants and GHGs emissions from 2016 to 2021.** With January 1, 2016,  
370 as the reference point, the five-day moving average of daily relative emissions is displayed.

371 To compare the magnitude of changes in emissions of various atmospheric pollutants and  
372 greenhouse gases emitted by ships, Fig. 4 converts the daily ship emissions of 9 species into daily relative  
373 quantities taking the emission levels on January 1, 2016, as the reference point. Figure 4 reveals that,  
374 aside from occasional sharp declines or increases on certain dates, the daily variations in ship emissions  
375 are generally stable. This suggests that the emission simulations by the SEIM model exhibit continuity  
376 and stability. Ships typically cruise at constant speeds on high seas without significant diurnal or other  
377 periodic variations, so global ship emissions do not exhibit pronounced daily or seasonal fluctuations.  
378 Any anomalies such as sudden drops or spikes may be attributed to signal transmission anomalies in  
379 equipment or meteorological factors. In 2019, the reduction in ship SO<sub>2</sub> emissions compared to 2018 was  
380 slightly larger than that of other pollutants, probably attributed to the implementation of the domestic  
381 emission control area policy within 12 nautical miles of the Chinese coast, one of the world's busiest  
382 areas for shipping activities (Chen et al., 2017), which has also been demonstrated by Fig. 7c.—From  
383 Fig. 4, finer temporal patterns can be observed, such as the gradual increase in emissions during the  
384 second half of 2017 and the subsequent decrease in ship emissions in 2019 as trade conflicts intensified.  
385 In 2020, the impact of the pandemic led to two phases of decline and recovery in global ship emissions.

386 The 2020 global fuel-switching policy also led to a significant reduction in ship SO<sub>2</sub>, PM<sub>2.5</sub>, and BC  
387 emissions. Despite the implementation of NECA policy from 2016 to 2021 (IMO, 2023), the decline in

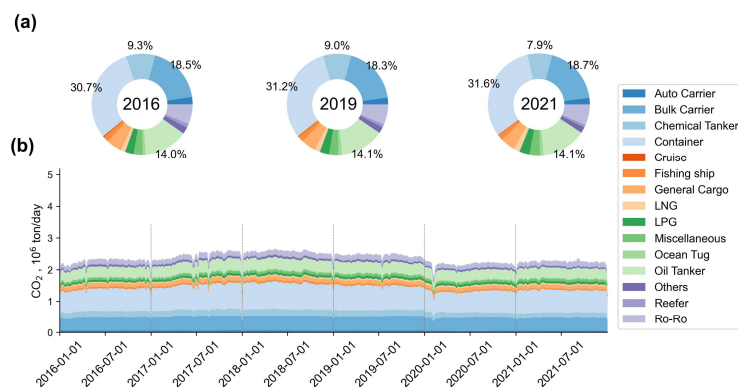
设置了格式: 下标

设置了格式: 下标

设置了格式: 字体: 倾斜, 下标

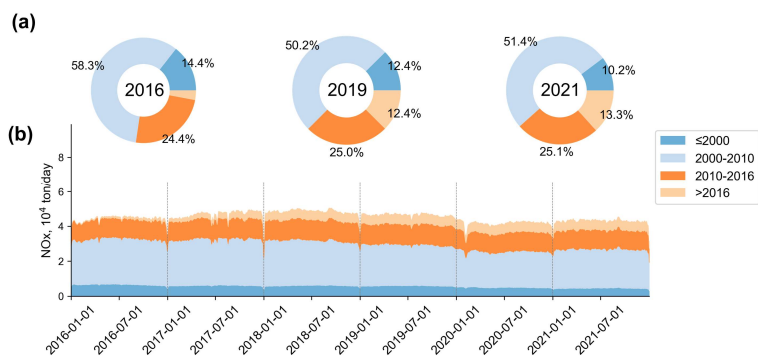
388 ship NO<sub>x</sub> emissions is very slow, as shown in Fig. 4, which is due to the fact that the current fleet is still  
389 predominantly composed of ships built before 2016 (accounting for more than 85%, as shown in Figure  
390 6). The slow pace of fleet renewal makes it more challenging to achieve substantial reductions in NO<sub>x</sub>  
391 emissions from ships currently. It is worth noting that CH<sub>4</sub> emissions exhibit relatively large daily  
392 changes and have been increasing throughout the six years. The primary source of CH<sub>4</sub> emissions is LNG  
393 ships. The daily fluctuations in ship CH<sub>4</sub> emissions are mainly due to variations in LNG ship activities.  
394 Although LNG ships are currently relatively few, their quantity is increasing as the demand for low-  
395 carbon ships grows steadily (Gronholm et al., 2021).

### 3.2.2 Multi-dimensional structure



397  
398 **Figure 5: Composition of global ship CO<sub>2</sub> emissions by vessel type from 2016 to 2021.** a) the percentage  
399 contribution of emissions by vessel type for the years 2016, 2019, and 2021; b) the five-day moving average of  
400 daily emissions for different vessel types.

401 Figure 5 displays the daily CO<sub>2</sub> emissions classified by vessel type. From 2016 to 2021, container  
402 ships, bulk carriers, and oil tankers consistently contributed the most, accounting for 31.6%, 18.7%, and  
403 14.1% of global ship CO<sub>2</sub> emissions in 2021, respectively. The contribution of container ships increased  
404 from 30.7% to 31.6% from 2016 to 2021. Overall, there were no significant changes in the composition  
405 of vessel types over the six years. Vessel types reflect the types of commodities transported by sea,  
406 indicating the relative stability of the global maritime cargo structure.



408

409 **Figure 6: Composition of global ship NO<sub>x</sub> emissions by vessel construction year from 2016 to 2021.** a) the  
 410 percentage contribution of emissions by vessels constructed in different periods for the years 2016, 2019, and 2021;  
 411 b) the five-day moving average of daily emissions for vessels constructed in different periods.

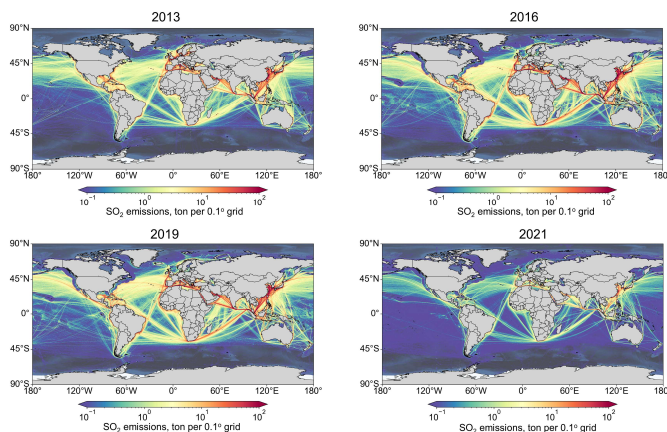
412 Figure 6 illustrates the daily NO<sub>x</sub> emissions composed by the vessel construction period. The  
 413 construction year of vessels determines the NO<sub>x</sub> emission standards followed by their engine (IMO,  
 414 2008). From 2016 to 2021, vessels complying with Tier I standards (built during the year 2000-2010)  
 415 consistently contributed over 50% of ship NO<sub>x</sub> emissions, while those complying with Tier II standards  
 416 (built during the year 2010-2015) contributed approximately half of Tier I emissions. As the majority of  
 417 ship NO<sub>x</sub> emissions come from Tier I- and Tier II-standard vessels, global ship NO<sub>x</sub> emissions are  
 418 expected to remain at current levels in the short term without further control measures. However, it is  
 419 noteworthy that the contribution of vessels over 20 years old (built-year ≤ 2000) to global ship NO<sub>x</sub>  
 420 emissions has gradually decreased, from 14.4% in 2016 to 10.2% in 2021. Meanwhile, the contribution  
 421 of newly built vessels (built-year ≥ 2016) to global ship NO<sub>x</sub> emissions has steadily increased from  
 422 3.5% in 2019 to 13.3% in 2021.

### 423 3.3 Spatial characteristics

#### 424 3.3.1 High-resolution patterns

425 Based on latitude and longitude coordinates in AIS signals, the ship emissions dataset was spatially  
 426 aggregated into grids, resulting in the global spatial distribution of ship emissions. Figure 7 depicts the  
 427 SO<sub>2</sub> emissions from global ships in 0.1° × 0.1° grids. The regions with high intensity of ship SO<sub>2</sub>  
 428 emissions include East Asia, South Asia, Europe, the Persian Gulf, the Mediterranean, and the western  
 429 coast of Europe. The intensive ship emissions along major global shipping routes are clearly visible, such

430 as the routes connecting East Asia through the Malacca Strait, the Suez Canal, and the Strait of Hormuz  
431 to Western European countries (the "Europe-Middle East-Far East route"), the Strait of Gibraltar, the  
432 Strait of Hormuz, and the critical passage connecting the Pacific and Atlantic Oceans, the Panama Canal,  
433 among others. Comparing the spatial distribution of ship SO<sub>2</sub> emissions in different years, noticeable  
434 reductions in emissions are observed in ECAs such as North America, the Gulf of Mexico, the North Sea,  
435 and the Baltic Sea comparing the ship SO<sub>2</sub> emissions distribution in 2013 and 2016. A significant  
436 reduction in emissions is also observed in the Domestic Emission Control Area (DECA) comparing the  
437 ship SO<sub>2</sub> emissions distribution in 2016 and 2019. In 2021, the implementation of the global low-sulfur  
438 fuel policy resulted in a significant overall reduction in ship SO<sub>2</sub> emissions spatially compared with 2019.  
439 The spatial distribution of ship SO<sub>2</sub> emissions in different years demonstrates that the SEIM v2.2  
440 effectively responds to SO<sub>2</sub> emission control policies.



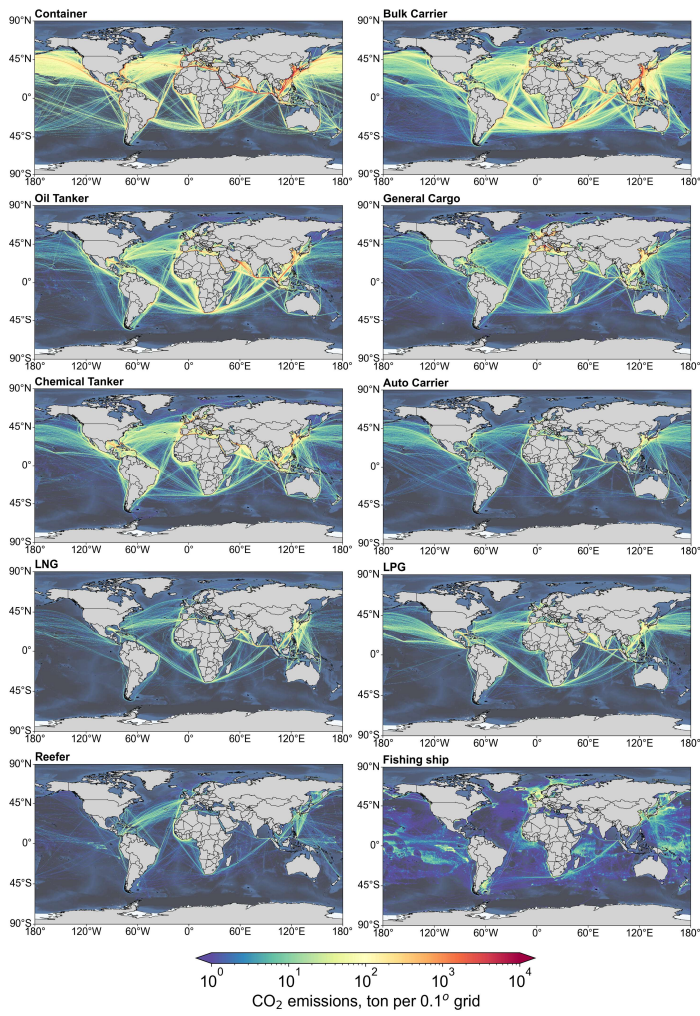
441

442 **Figure 7: Spatial distribution of global ship SO<sub>2</sub> emissions in different years**

### 443 3.3.2 Spatial disparities of vessel composition

444 Distinct disparities in spatial distribution are evident between freight vessels and non-freight  
445 vessels in Fig. 8. Emissions from container ships, bulk carriers, and oil tankers are concentrated in major  
446 international shipping lanes. In contrast, emissions from non-transport vessels such as fishing vessels are  
447 more widely distributed in non-lane open sea areas. According to this study, in 2021, fishing vessels  
448 contributed 1.6% to global ship CO<sub>2</sub> emissions, with their emissions mainly concentrated in the North  
449 Sea, Baltic Sea, Yellow Sea, and South Pacific. In recent years, studies have utilized fine satellite data to

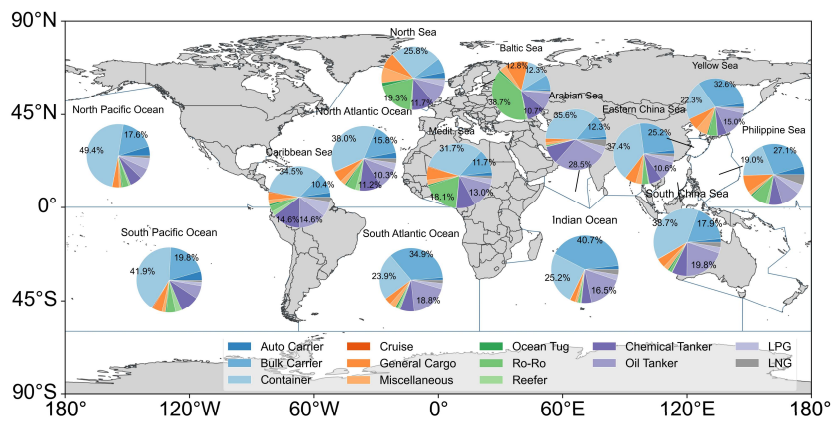
450 reveal significant fishing vessel activities that had not been publicly tracked worldwide (Paolo et al.,  
451 2024). The emissions from those fishing vessels remain unknown. Therefore, the emissions from fishing  
452 vessels presented in this study should be considered highly uncertain and are not discussed in the  
453 following sections.



454

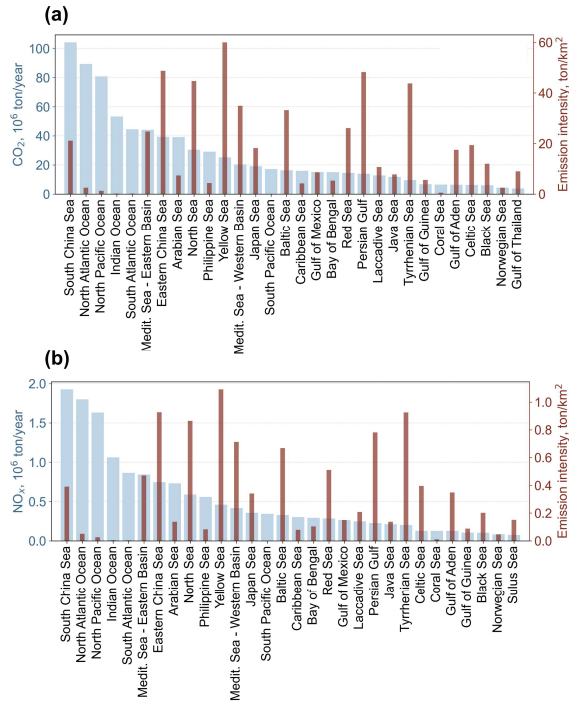
455 **Figure 8: Spatial distribution of CO<sub>2</sub> emissions from different types of vessels in 2021**

456 The spatial distribution of emissions varies across different vessel types, leading to disparities in the  
 457 composition of vessel types in different maritime regions. The division of global maritime regions is  
 458 based on the International Hydrographic Organization (IHO) standards (<https://iho.int/>). Figure 9  
 459 illustrates the composition of vessel types in the top 14 regions with the highest CO<sub>2</sub> emissions globally  
 460 in 2021, with their combined emissions accounting for almost 80% of the total global emissions. In the  
 461 pie charts for each region, vessel types contributing over 10% of emissions are labeled. It is observed  
 462 that container ships contribute significant emissions in the North Pacific Ocean, South China Sea, and  
 463 East China Sea, accounting for 49.4%, 37.4%, and 38.7% respectively, well above the global average  
 464 (31.6%). Regions with high contributions from bulk carriers are mainly distributed in the southern  
 465 hemisphere, such as the Indian Ocean (40.7%) and South Atlantic (34.9%). Ro-Ro vessels exhibit high  
 466 emissions proportions near Europe, with percentages of 38.7% in the Baltic Sea, 19.3% in the North Sea,  
 467 and 18.1% in the Mediterranean. Oil tankers contribute 28.5% of emissions in the Arabian Sea, probably  
 468 attributed to countries like Saudi Arabia and Iran, rich in oil and gas resources, generating substantial  
 469 shipping emissions during exports to other countries.



470  
 471 **Figure 9: Ship CO<sub>2</sub> emissions composition in different maritime regions globally in 2021 (excluding fishing**  
 472 **ships and others)**

473 **3.3.3 Emission intensity**



474 **Figure 10: Global ship (a) CO<sub>2</sub> and (b) NO<sub>x</sub> emission and emission intensities in different maritime regions**  
 475 **in 2021**  
 476

477 Since the significant differences in the area of  $0.1^\circ \times 0.1^\circ$  grids at different latitudes, ship emissions  
 478 within each grid are standardized into emission intensity, i.e., emissions per unit area (unit: ton/km<sup>2</sup>).  
 479 Taking ship CO<sub>2</sub> emissions as an example, Fig. 10 illustrates the total ship CO<sub>2</sub> emissions and emission  
 480 intensity in major maritime regions in 2021. The top 30 maritime regions with the highest CO<sub>2</sub> and NO<sub>x</sub>  
 481 emissions, accounting for approximately 96% of the total global ship emissions, are listed and arranged  
 482 in descending order of total emissions. It is important to note that the South/North Pacific, South/North  
 483 Atlantic, and Indian Ocean cover a vast area (about 75% of the total maritime area), most of which have  
 484 little or no ship navigation. Calculating the total average emission intensity for these regions would  
 485 weaken their significance, so they are not discussed here. Among other maritime regions, the South China  
 486 Sea has the highest total ship CO<sub>2</sub> and NO<sub>x</sub> emissions. As a vital route for maritime trade between East  
 487 Asia Europe and Africa, the South China Sea exhibits prominent ship traffic density globally.



488 Additionally, the Eastern Mediterranean Basin, the Arabian Sea, the East China Sea, the Philippine Sea,  
489 and the North Sea also have relatively significant total emissions. Generally, maritime regions with high  
490 CO<sub>2</sub> emissions also have relatively high NO<sub>x</sub> emissions. Although the order of maritime regions with  
491 lower emissions differs slightly, overall consistency is observed. There are significant differences  
492 between maritime regions with high emissions and those with high emission intensity. The top five  
493 maritime regions with the highest ship CO<sub>2</sub> emission intensity are the Yellow Sea, the Persian Gulf, the  
494 East China Sea, the North Sea, and the Tyrrhenian Sea. The top five for NO<sub>x</sub> emission intensity are also  
495 the same maritime regions. These regions are coastal areas or busy maritime routes with intensive ship  
496 emissions, which warrants attention in environmental management in the future.

#### 497 **4 Data Availability**

498 Shipping emission data described in this manuscript can be accessed at Zenodo under  
499 <https://zenodo.org/records/11069531> (Wen et al., 2024).

#### 500 **5 Conclusions**

501 Utilizing the SEIM model, we developed a high-resolution ship emission inventory covering the  
502 period from 2013 to 2016-2021 globally, encompassing 5 atmospheric pollutants (NO<sub>x</sub>, SO<sub>2</sub>, PM<sub>2.5</sub>, CO,  
503 HC) and 4 greenhouse gases (CO<sub>2</sub>, CH<sub>4</sub>, N<sub>2</sub>O, BC). With a temporal resolution of day and spatial  
504 resolution of 0.1° × 0.1°, our inventory revealed novel insights into global ship emission characteristics.

505 In terms of annual emissions, our inventory exhibits consistency in temporal trends and emission  
506 magnitudes compared to mainstream inventory datasets including EDGAR, CEDS, and IMO. According  
507 to this study and the global anthropogenic emission inventory by (Hoesly Rachel, 2024), ship emissions  
508 contributed 12.3% of SO<sub>2</sub>, 14.0% of NO<sub>x</sub>, and 2.5% of CO<sub>2</sub> to global anthropogenic emissions in 2019,  
509 and 3.2% of SO<sub>2</sub>, 14.2% of NO<sub>x</sub>, and 2.3% of CO<sub>2</sub> to global anthropogenic emissions in 2021. Over the  
510 years, ship CO<sub>2</sub>, NO<sub>x</sub>, CO, HC, and N<sub>2</sub>O emissions showed a declining trend due to the impacts of the  
511 2019 trade conflict (year-on-year decrease rate 5.4%-6.2%) and the 2020 pandemic (year-on-year  
512 decrease rate 7.4%-13.8%), with a subsequent rebound in 2021 as international trade increased (year-on-  
513 year increase rate 3.1%-3.6%). SO<sub>x</sub>, PM, and BC emissions were significantly influenced by gradually

514 implemented ECA policies and the 2020 low-sulfur fuel-switching policy. SO<sub>x</sub> and PM emissions in  
515 2021 were 80.9% and 76.0% of those in 2019, and BC emissions were 38.7% of those in 2019. CH<sub>4</sub>  
516 emissions exhibited an increasing trend over the years, growing by 43.5% in 2021 compared to 2016.

517 Regarding emission composition, container ships consistently constituted the primary source of  
518 global ship CO<sub>2</sub> emissions, contributing over 30% annually and steadily increasing, followed by bulk  
519 carriers, oil tankers, and chemical tankers. The proportion of emissions contributed by new ships  
520 increased annually from 3.5% in 2016 to 13.3% in 2021. However, Tier I and Tier II ships still dominate  
521 ship NO<sub>x</sub> emissions. Currently, Tier III standards only apply to vessels operating in North American  
522 Emission Control Areas. Achieving a significant reduction in global ship NO<sub>x</sub> emissions still requires  
523 extensive advancements in ship engine technology and follow-up regulatory measures worldwide.

524 As for spatial characteristics, ship emissions were particularly significant in East Asia, South Asia,  
525 and Europe, with busy shipping routes such as the Western Europe-Middle East-Far East route, the Strait  
526 of Malacca, the Strait of Gibraltar, the Strait of Hormuz, and the Panama Canal showing the highest  
527 emission intensities. The regions with the highest CO<sub>2</sub> and NO<sub>x</sub> ship emission intensities were the Yellow  
528 Sea, the Persian Gulf, the East China Sea, the North Sea, and the Tyrrhenian Sea. These are not only  
529 areas with the highest emission intensity but also coastal regions with dense populations and ecosystems  
530 vulnerable to pollution. This suggests that these regions should be prioritized in environmental  
531 management efforts for improving air quality, protecting marine ecosystems, and climate mitigation.  
532 Furthermore, influenced by the types of commodities transported and the countries involved in trade,  
533 significant differences in ship emission characteristics exist across different regions. SEIM enables the  
534 analysis of the heterogeneity of spatial distributions of ship emissions. In terms of vessel type  
535 composition, container ships significantly exceeded the global average in ship CO<sub>2</sub> emissions  
536 contributions in the North Pacific, East China Sea, and South China Sea. Regions with high proportions  
537 of emissions from bulk carriers were mainly located in the Southern Hemisphere, such as the Indian  
538 Ocean, South Pacific, and South Atlantic. Emissions from oil tankers were high in the Arabian Sea and  
539 the Persian Gulf. The regions with the highest CO<sub>2</sub> and NO<sub>x</sub> ship emission intensities were the Yellow  
540 Sea, the Persian Gulf, the East China Sea, the North Sea, and the Tyrrhenian Sea. The findings on the  
541 spatial heterogeneity of global ship emissions offer insights into region-specific management. In addition,  
542 since many high-emission regions include transboundary areas, such as the South China Sea and the

543 Mediterranean, where maritime traffic connects multiple countries., effective mitigation in these regions  
544 will require international cooperation.

545 Although the complex quality control processes employed in this study, uncertainties still persist  
546 in the aspects of AIS data accuracy, emission factors and so on. In the next steps, more work should be  
547 done to reduce the uncertainties in bottom-up ship emission evaluation model, including integrating latest  
548 methods and multi-source data to improve the accuracy of AIS data quality control, gathering more  
549 studies on recent ship emission factors to cover more ship size and operating status, as well as involving  
550 multiple data sources such as satellite data to validate the results.

551 Overall, SEIM offers a globally multi-year, high spatiotemporal resolution ship emission inventory  
552 that provides reliable and detailed data, which could support foundational research across disciplines  
553 such as atmospheric science, environmental science, and geoscience. Meanwhile, this dataset could also  
554 provide scientific support for facilitating shipping emission mitigation in the future.

555

#### 556 **Acknowledgments**

557 This work was supported by the National Natural Science Foundation of China (grant nos. 42325505),  
558 National Key Research and Development Program of China (No. 2023YFC3705604 and No.  
559 2022YFC3704200), and China Postdoctoral Science Foundation (No. 2023M730142).

#### 560 **Author contributions**

561 W.Y. and X.W. designed the research and wrote the manuscript, H.L. reviewed and revised the  
562 manuscript, and T.H. contributed to the modelling. Z.L. and Z.L. contributed to data analysis. K.H. and  
563 H.L. provided insights into the research design. All authors contributed to the writing. We also thank  
564 Harvard-China Project on Energy, Economy and Environment and Professor Chris P. Nielsen from  
565 Harvard University, for his suggested revisions to this manuscript.

#### 566 **Competing interests**

567 The authors declare no competing interests.

带格式的: 缩进: 首行缩进: 2 字符

568 **References**

- 569 Browse, J., Carslaw, K. S., Schmidt, A., and Corbett, J. J.: Impact of future Arctic shipping on high-  
570 latitude black carbon deposition, *Geophysical Research Letters*, 40, 4459-4463,  
571 <https://doi.org/10.1002/grl.50876>, 2013.
- 572 Chen, D., Wang, X., Li, Y., Lang, J., Zhou, Y., Guo, X., and Zhao, Y.: High-spatiotemporal-resolution  
573 ship emission inventory of China based on AIS data in 2014, *Science of The Total Environment*, 609,  
574 776-787, 10.1016/j.scitotenv.2017.07.051, 2017.
- 575 Chen, D., Fu, X., Guo, X., Lang, J., Zhou, Y., Li, Y., Liu, B., and Wang, W.: The impact of ship emissions  
576 on nitrogen and sulfur deposition in China, *Science of The Total Environment*, 708, 134636,  
577 <https://doi.org/10.1016/j.scitotenv.2019.134636>, 2020.
- 578 Chen, X. and Yang, J.: Analysis of the uncertainty of the AIS-based bottom-up approach for estimating  
579 ship emissions, *Marine Pollution Bulletin*, 199, 115968,  
580 <https://doi.org/10.1016/j.marpolbul.2023.115968>, 2024.
- 581 Corbett, J. J., Fischbeck, P. S., and Pandis, S. N.: Global nitrogen and sulfur inventories for oceangoing  
582 ships, *Journal of Geophysical Research: Atmospheres*, 104, 3457-3470, 10.1029/1998jd100040, 1999.
- 583 Crippa, M., Guizzardi, D., Solazzo, E., Muntean, M., Schaaf, E., Monforti-Ferrario: GHG emissions of  
584 all world countries - 2021 Report, Luxembourg, 2021.
- 585 Development, t. U. N. C. o. T. a.: Review of Maritime Transport, 2023.
- 586 Diamond, M. S.: Detection of large-scale cloud microphysical changes within a major shipping corridor  
587 after implementation of the International Maritime Organization 2020 fuel sulfur regulations, *Atmos.*  
588 *Chem. Phys.*, 23, 8259-8269, 10.5194/acp-23-8259-2023, 2023.
- 589 DNV: Maritime Forecast to 2050, 2022.
- 590 Emmens, T., Amrit, C., Abdi, A., and Ghosh, M.: The promises and perils of Automatic Identification  
591 System data, *Expert Systems with Applications*, 178, 114975,  
592 <https://doi.org/10.1016/j.eswa.2021.114975>, 2021.
- 593 Endresen, O., Sorgard, E., Sundet, J. K., Dalsoren, S. B., Isaksen, I. S. A., Berglen, T. F., and Gravir, G.:  
594 Emission from international sea transportation and environmental impact, *Journal of Geophysical*  
595 *Research-Atmospheres*, 108, 10.1029/2002jd002898, 2003.
- 596 Eyring, V., Isaksen, I. S. A., Berntsen, T., Collins, W. J., Corbett, J. J., Endresen, O., Grainger, R. G.,  
597 Moldanova, J., Schlager, H., and Stevenson, D. S.: Transport impacts on atmosphere and climate:  
598 Shipping, *Atmospheric Environment*, 44, 4735-4771, 10.1016/j.atmosenv.2009.04.059, 2010.
- 599 Fu, M., Liu, H., Jin, X., and He, K.: National- to port-level inventories of shipping emissions in China,  
600 *Environmental Research Letters*, 12, 10.1088/1748-9326/aa897a, 2017.
- 601 Fu, X., Chen, D., Guo, X., Lang, J., and Zhou, Y.: Improving the estimation of ship emissions using the  
602 high-spatiotemporal resolution wind fields simulated by the Weather Research and Forecast model: A  
603 case study in China, *Journal of Industrial Ecology*, 26, 1871-1881, <https://doi.org/10.1111/jiec.13278>,  
604 2022.
- 605 Gronholm, T., Makela, T., Hatakka, J., Jalkanen, J. P., Kuula, J., Laurila, T., Laakso, L., and Kukkonen,  
606 J.: Evaluation of Methane Emissions Originating from LNG Ships Based on the Measurements at a  
607 Remote Marine Station, *Environ Sci Technol*, 55, 13677-13686, 10.1021/acs.est.1c03293, 2021.
- 608 Hoesly Rachel, S. S.: CEDS v\_2024\_04\_01 Release Emission Data (v\_2024\_04\_01) Zenodo [dataset],  
609 <https://doi.org/10.5281/zenodo.10904361>, 2024.

610 IMO: Emission Control Areas (ECAs) designated under MARPOL Annex VI.  
611 IMO: Amendments to the technical code on control of emission of nitrogen oxides from marine diesel  
612 engines, 2008.  
613 IMO: Further technical and operational measures for enhancing the energy efficiency of international  
614 shipping, 2015.  
615 Jalkanen, J. P., Johansson, L., Kukkonen, J., Brink, A., Kalli, J., and Stipa, T.: Extension of an assessment  
616 model of ship traffic exhaust emissions for particulate matter and carbon monoxide, *Atmospheric  
617 Chemistry and Physics*, 12, 2641-2659, 10.5194/acp-12-2641-2012, 2012.  
618 Jasper Faber, S. H., Shuang Zhang, Paula Pereda, Bryan Comer: Forth IMO Greenhouse gas study,  
619 London, 2020.  
620 Johansson, L., Jalkanen, J.-P., and Kukkonen, J.: Global assessment of shipping emissions in 2015 on a  
621 high spatial and temporal resolution, *Atmospheric Environment*, 167, 403-415,  
622 10.1016/j.atmosenv.2017.08.042, 2017.  
623 Kersey, J., Popovich, N. D., and Phadke, A. A.: Rapid battery cost declines accelerate the prospects of  
624 all-electric interregional container shipping, *Nature Energy*, 7, 664-674, 10.1038/s41560-022-01065-y,  
625 2022.  
626 Kramel, D., Muri, H., Kim, Y., Lonka, R., Nielsen, J. B., Ringvold, A. L., Bouman, E. A., Steen, S., and  
627 Strømman, A. H.: Global Shipping Emissions from a Well-to-Wake Perspective: The MariTEAM Model,  
628 *Environmental Science & Technology*, 55, 15040-15050, 10.1021/acs.est.1c03937, 2021.  
629 Liu, H., Fu, M., Jin, X., Shang, Y., Shindell, D., Faluvegi, G., Shindell, C., and He, K.: Health and climate  
630 impacts of ocean-going vessels in East Asia, *Nature Climate Change*, 6, 1037-1041,  
631 10.1038/nclimate3083, 2016.  
632 Liu, H., Yi, W., Jalkanen, J.-P., Luo, Z., Majamäki, E., Matthias, V., Moldanová, J., Shi, Z., and He, K.:  
633 Atmospheric impacts and regulation framework of shipping emissions: achievements, challenges and  
634 frontiers, *Fundamental Research*, <https://doi.org/10.1016/j.fmre.2024.02.013>, 2024.  
635 Luo, Z., He, T., Yi, W., Zhao, J., Zhang, Z., Wang, Y., Liu, H., and He, K.: Advancing shipping NOx  
636 pollution estimation through a satellite-based approach, *PNAS Nexus*, pgad430,  
637 10.1093/pnasnexus/pgad430, 2023.  
638 Luo, Z., Lv, Z., Zhao, J., Sun, H., He, T., Yi, W., Zhang, Z., He, K., and Liu, H.: Shipping-related  
639 pollution decreased but mortality increased in Chinese port cities, *Nature Cities*, 1, 295-304,  
640 10.1038/s44284-024-00050-8, 2024.  
641 McDuffie, E. E., Smith, S. J., O'Rourke, P., Tibrewal, K., Venkataraman, C., Marais, E. A., Zheng, B.,  
642 Crippa, M., Brauer, M., and Martin, R. V.: A global anthropogenic emission inventory of atmospheric  
643 pollutants from sector- and fuel-specific sources (1970–2017): an application of the Community  
644 Emissions Data System (CEDS), *Earth System Science Data*, 12, 3413-3442, 10.5194/essd-12-3413-  
645 2020, 2020.  
646 Paolo, F. S., Kroodsma, D., Raynor, J., Hochberg, T., Davis, P., Cleary, J., Marsaglia, L., Orofino, S.,  
647 Thomas, C., and Halpin, P.: Satellite mapping reveals extensive industrial activity at sea, *Nature*, 625,  
648 85-91, 10.1038/s41586-023-06825-8, 2024.  
649 Smith, T. W. P. J., J. P.; Anderson, B. A.; Corbett, J. J.; Faber, J.; Hanayama: Third IMO GHG Study,  
650 London, 2014.

651 Sou, W. S., Goh, T., Lee, X. N., Ng, S. H., and Chai, K.-H.: Reducing the carbon intensity of international  
652 shipping – The impact of energy efficiency measures, *Energy Policy*, 170, 10.1016/j.enpol.2022.113239,  
653 2022.

654 Stephenson, S. R., Wang, W., Zender, C. S., Wang, H., Davis, S. J., and Rasch, P. J.: Climatic Responses  
655 to Future Trans-Arctic Shipping, *Geophys Res Lett*, 45, 9898-9908, 10.1029/2018GL078969, 2018.

656 Wang, X., Yi, W., Lv, Z., Deng, F., Zheng, S., Xu, H., Zhao, J., Liu, H., and He, K.: Ship emissions  
657 around China under gradually promoted control policies from 2016 to 2019, *Atmospheric Chemistry and  
658 Physics*, 21, 13835-13853, 10.5194/acp-21-13835-2021, 2021.

659 Wen, Y., Xiaotong, W., Tingkun, H., Huan, L., Luo, Z., and Kebin, H.: Global shipping emissions for  
660 the years 2013 and 2016-2021, *Zenodo [dataset]*, 10.5281/zenodo.10869014, 2024.

661 Yuan, T., Song, H., Wood, R., Wang, C., Oreopoulos, L., Platnick, S. E., von Hippel, S., Meyer, K.,  
662 Light, S., and Wilcox, E.: Global reduction in ship-tracks from sulfur regulations for shipping fuel,  
663 *Science Advances*, 8, eabn7988, 10.1126/sciadv.abn7988, 2022.

664 Zhang, C., Shi, Z., Zhao, J., Zhang, Y., Yu, Y., Mu, Y., Yao, X., Feng, L., Zhang, F., Chen, Y., Liu, X.,  
665 Shi, J., and Gao, H.: Impact of air emissions from shipping on marine phytoplankton growth, *Science of  
666 The Total Environment*, 769, 145488, <https://doi.org/10.1016/j.scitotenv.2021.145488>, 2021.

667 Zhang, Q., Wan, Z., Hemmings, B., and Abbasov, F.: Reducing black carbon emissions from Arctic  
668 shipping: Solutions and policy implications, *Journal of Cleaner Production*, 241,  
669 10.1016/j.jclepro.2019.118261, 2019.

670

671